Applied Catalysis B: Environmental 158–159 (2014) 280–285

Contents lists available at ScienceDirect

Applied Catalysis B: Environmental

journal homepage: www.elsevier.com/locate/apcatb

Factors impacted on anisotropic photocatalytic oxidization activity of ZnO: Surface band bending, surface free energy and surface conductance

Guoqiang Li[a,b], Zhiguo Yi[c], Hongtao Wang[a,b], Caihong Jia[a,b], Weifeng Zhang[a,*]

[a] Key Laboratory of Photovoltaic Materials of Henan Province and School of Physics & Electronics, Henan University, Kaifeng 475004, PR China
[b] Institute of Physics for Microsystems, Henan University, Kaifeng 475004, PR China
[c] Fujian Institute of Research on the Structure of Matter, Chinese Academy of Sciences, Fuzhou, Fujian 350002, PR China

ARTICLE INFO

Article history:
Received 24 February 2014
Received in revised form 16 April 2014
Accepted 19 April 2014
Available online 30 April 2014

Keywords:
ZnO
Photocatalysis
Crystal plane
Anisotropy

ABSTRACT

ZnO thin films with three low-indexed crystal planes were prepared by pulsed laser deposition and investigated for photocatalytic activity. The results revealed that the ZnO showed anisotropic photocatalytic activity and the order of activity for methylene orange and dichlorophene decomposition was (0 0 1)<(1 0 0)<(1 1 0). The highest photocatalytic activity of the (1 1 0) crystal plane orientated sample was ascribed to the more upward surface band bending, higher surface free energy and larger surface conductance. These results implied that synthesizing the (1 1 0) facet exposed ZnO sample would be an effective approach for the obtainment of higher activity.

1. Introduction

Semiconductor photocatalysis has attracted much attention due to the extensive potential applications in renewable energy production and environmental remediation [1]. Many semiconductor oxides including ZnO were extensively studied for the photocatalytic activity [2–10]. For example, Jang et al. investigated the nanoplate, nanorod, microrod and dumbbell-shaped microrod of ZnO and found that the nanoplate with a high population of polar ZnO (0 0 1) faces showed the highest photocatalytic activity for H_2O_2 generation [6]. Mclaren et al. observed that the photocatalytic activity for methylene blue (MB) degradation over the ZnO nanoparticles increased with the rise in the ratio of (1 0 0)/(0 0 2) [8]. These previous studies got the different conclusions on the effect of polar (0 0 1) plane and nonpolar (1 0 0). It was noted that all the samples were particles which contained at least two kinds of crystal facets. Tachikawa et al. found that there was the electron transfer from the (0 0 1) to (1 0 1) in the TiO_2 particle with the well-defined facets [11]. Therefore, the conflict in the activity of ZnO might come from the electron transfer between the different crystal facets. To obtain the exact activity of the certain crystal plane, the sample only containing one specific plane should be investigated. Kislov et al. reported the photocatalytic activity for methylene orange (MO) degradation over the single crystal ZnO with (1 0 0) plane was higher than that with (0 0 1) plane [7]. Miyauchi et al. investigated the photoinduced hydrophilicity of heteroepitaxially grown ZnO thin films on *a*-plane, *c*-plane and *r*-plane sapphire prepared by rf-magnetron sputtering and found that the ZnO film oriented along the (1 1 0) direction exhibited a higher hydrophilicizing rate than those oriented along the (0 0 1) direction [12]. However, ZnO with the wurtzite structure had three low-indexed crystal planes, namely polar (0 0 1), and nonpolar (1 0 0) and (1 1 0), as shown in Fig. 1I. Further investigation on the activity of given plane of ZnO photocatalyst was important for the understanding of the origin of photocatalytic activity and selectivity.

In this study, the ZnO thin films with three low-indexed crystal planes were prepared on *a*-plane, *m*-plane and *r*-plane sapphire by pulsed laser deposition (PLD) and investigated for photocatalytic activity. The order of photocatalytic activity of ZnO with the (0 0 1), (1 0 0) and (1 1 0) crystal plane was obtained. The origins for this order were discussed based on the characteristics of the optical properties, band structure, surface properties (morphology, composition and surface energy) and photoelectrical property.

* Corresponding author. Tel.: +86 378 3881 940; fax: +86 378 3880 659.
E-mail address: wfzhang@henu.edu.cn (W. Zhang).

http://dx.doi.org/10.1016/j.apcatb.2014.04.034
0926-3373/

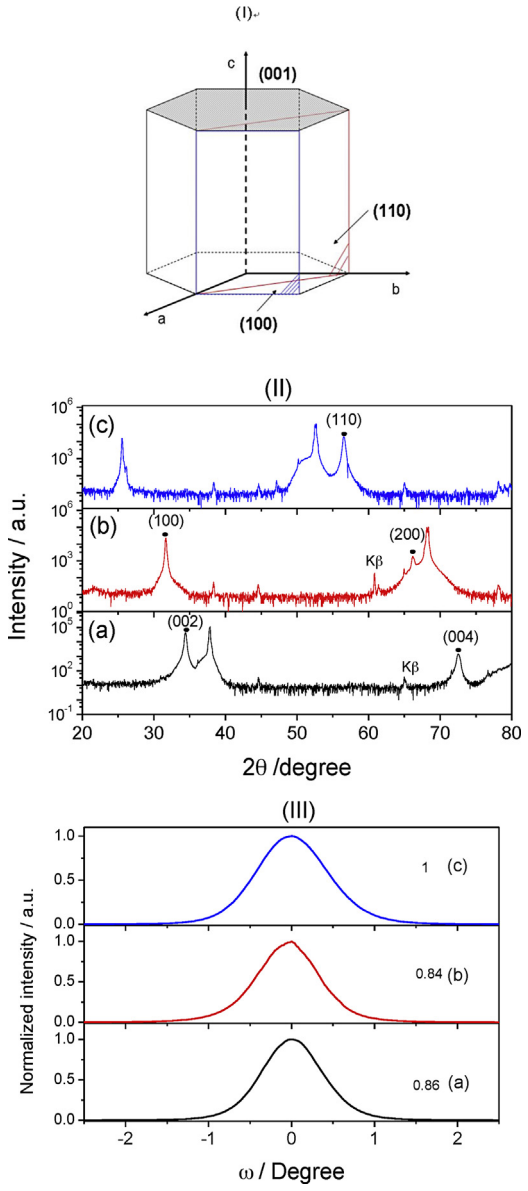

Fig. 1. Schematic of wurtzite structure of ZnO with (0 0 1), (1 0 0) and (1 1 0) crystal planes (I). X-ray diffraction (XRD) patterns (II) and ω-scan spectra (III) of ZnO thin films grown on *a*-plane (a), *m*-plane (b) and *r*-plane (c) sapphire.

2. Experimental

2.1. Sample preparation

The ZnO thin films were deposited on *a*-plane, *m*-plane and *r*-plane sapphire substrates by PLD. The fabrication conditions for the ZnO layer were as follows: laser repetition rate 3 Hz, target and substrate distance 50 mm, laser energy of 300 mJ, O_2 partial pressure about 2.0×10^{-2} Pa, substrate temperature 873 K, and deposited time 0.5 h.

2.2. Material characterization

The thicknesses of ZnO thin films grown on *a*-plane, *m*-plane and *r*-plane sapphire were estimated with the aid of ellipsometer (type II, Taijing Tuopu Co., China) with a light source of He–Ne laser ($\lambda = 632$ nm). The crystal structures of samples were determined by an X-ray diffractometer (DX-2500 diffractometer, Fangyuan) with Cu Kα radiation ($\lambda = 0.154145$ nm) in θ–2θ mode. The carrier density was obtained from the Hall measurement. The surface morphology was observed by atomic force microscopy (AFM, SPA400, Japan) and a scanning electron microscopy (SEM, JSM-7001F, JEOL Ltd.). The transmittance spectrum was recorded with a UV-Vis spectrophotometer (Varian Cary 5000) using air as the reference and transformed to the absorption spectra automatically. In the case of X-ray photoelectron spectroscopy (Thermo ESCALAB 250, USA), an Al anode with a monochromator was used to reduce the background signal. The binding energy was referenced to the C 1s peak taken at 284.8 eV. Valance band X-ray photoelectron spectroscopy (VB-XPS) was used to determine the top of valence band. Raman scattering spectrum was measured using a laser Raman spectrophotometer (RM-1000, Renishaw). Surface conductivity was measured on the samples covered by the plane fork electrode with the fork width of 0.1 mm under full arc of 450-W Xe lamp irradiation.

2.3. Evaluation of photocatalytic activity

The photocatalytic activities of the as-prepared samples were evaluated by the MO and 2,4-dichlorophene (DCP) photodegradation under full arc irradiation of 300-W Xe lamp, the spectrum of which was the same as our reported previously [13]. The light intensity was 290 mW/cm^2. The photocatalytic reaction was carried out over the samples with the 1 cm^2 area in a 1 ml MO or DCP solution in a sealed quartz cuvette with the light path length of 3 mm. There is no stirring during irradiation, but shaking before measuring the absorbance. The initial concentration of MO solution was 10 mg L^{-1} and the DCP is 4.8 mg L^{-1} which was the saturation solution at 20 °C. After 30-min dark-reaction, the absorption spectra variations of the MO and DCP were in-situ recorded at the intervals of 10 min using a UV-Vis spectrophotometer (UV2550, Shimadzu, Japan).

3. Results and discussion

The X-ray diffraction (XRD) patterns of ZnO thin films grown on *a*-plane, *m*-plane and *r*-plane sapphire were shown in Fig. 1II. Obviously, the oriented ZnO films were fabricated successfully. All peaks belonging to ZnO were marked, and the other peaks belonged to the substrate. The oriented ZnO film with polar plane of (0 0 2) was observed on *a*-plane sapphire. The lattice parameter along the *c*-axis for this ZnO film was 5.2096 Å. The ZnO thin films grown on *m*-plane and *r*-plane sapphire oriented the nonpolar plane (1 0 0) and (1 1 0), which was similar to the previous reports [14,15]. The lattice parameter along the *a*-axis was 3.2598 Å for the sample with (1 0 0) orientation and 3.2528 Å for that with (1 1 0) orientation. For simplicity, hereafter, the samples on *a*-plane, *m*-plane and *r*-plane sapphire were denoted as *A*(0 0 1), *B*(1 0 0) and *C*(1 1 0), respectively. The crystal qualities of all the samples were characterized by the ω-scan spectra, as shown in Fig. 1III. The full width at half maximum (FWHM) was 0.86° for A(0 0 1), 0.84° for B(1 0 0) and 1° for C(1 1 0), which was similar to the previous results obtained from the samples prepared by PLD [16]. Additionally, the thicknesses of *A*(0 0 1), *B*(1 0 0) and *C*(1 1 0) were estimated to be 268, 273 and 285 nm, respectively, indicating that they had the similar deposition rate.

Photocatalytic activities for the decomposition of MO and DCP in an aqueous solution were evaluated in the presence of ZnO films under full arc irradiation of Xe lamp. The reaction, monitored at 464 nm for MO and 198 nm for DCP (see Fig. S1 in Supporting information), followed pseudo-first order reaction kinetics for all the samples. When the reagent solution was dilute, the reaction rate (r) could be expressed as $r = kKC$, where, K refers to adsorption equilibrium constant, k is the apparent rate constant, and C is the instantaneous concentration of the reactant. The apparent rate

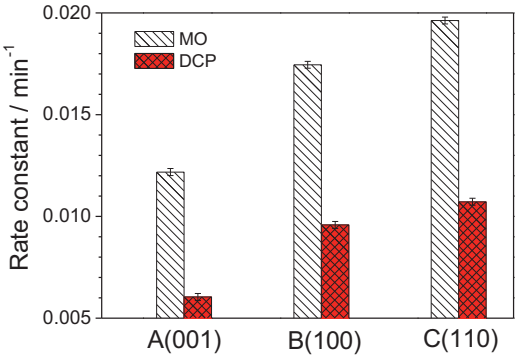

Fig. 2. Variation in rate constant in the degradation of MO (black) and DCP (red) over $A(0\,0\,1)$, $B(1\,0\,0)$ and $C(1\,1\,0)$. The error bar of 1.7×10^{-4} was obtained from the standard deviation of three reaction cycles of RhB degradation. (For interpretation of the references to color in this figure legend, the reader is referred to the web version of the article.)

constant for MO and DCP were calculated (see Fig. S2 in Supporting information) and drawn in Fig. 2. The increasing order of activity for both MO and DCP was $A(0\,0\,1) < B(1\,0\,0) < C(1\,1\,0)$. The rate constant for MO was 0.0196 min^{-1} for $C(1\,1\,0)$, which was 160% larger than $A(0\,0\,1)$. Kislov and Mclaren found that the $(1\,0\,0)$ plane was more active in the degradation of dye than the $(0\,0\,1)$ plane, [7,8] which was consistent with our result. However, Jang et al. found that the nanoplates with a high population of polar Zn $(0\,0\,1)$ faces showed the highest photocatalytic activity for H_2O_2 generation [6]. These conflicts were possibly caused by the different mechanisms as bulk and surface might posses different properties [9]. To clarify this, we further examined the optical properties, band structure, surface properties (morphology, composition and surface energy) and electrical property of the prepared thin film samples.

All of the prepared samples showed ultraviolet light absorption, as displayed in Fig. 3a. The optical band gap was estimated from UV–vis spectrum to be 3.26 eV for $A(0\,0\,1)$, 3.29 eV for $B(1\,0\,0)$, 3.30 eV for $C(1\,1\,0)$, see the inset of Fig. 3a. This difference might be attributed to the surface induced defects which modulate the band-gap transitions in ZnO [17,18]. The $A(0\,0\,1)$ had the smallest band gap, but showed the lowest photocatalytic activity. Based on the principle of photocatalysis, the sample with small band gap could absorb more photons, generate more e–h pairs, leading to a higher activity. However, our observation was opposite to above speculation. Consequently, we thought some important factor should be there except for the band gap. Moreover, $A(0\,0\,1)$ showed an absorption tail which extended over 400 nm. It could be attributed to the defects because it contained the most amount of defect, as discussed later.

The band position was closely related to the photocatalytic activity [19–21]. The VB top estimated from the VB-XPS was 3.16 eV for $A(0\,0\,1)$, 2.95 eV for $B(1\,0\,0)$, 2.77 eV for $C(1\,1\,0)$, see Fig. 3b. Yang et al. found that the VB top of the ZnO along $(0\,0\,1)$ on *c*-plane sapphire and along $(1\,1\,0)$ on *r*-plane sapphire prepared by low-pressure metal-organic chemical vapor deposition (MOCVD) located at 2.43 and 2.29 eV, respectively [22]. Moreover, Allen et al. reported that the VB top of ZnO single crystal along $(1\,0\,0)$ prepared by hydrothermal method and along $(1\,1\,0)$ prepared by pressurized-melt method was at 3.60 and 3.54 eV [23]. The

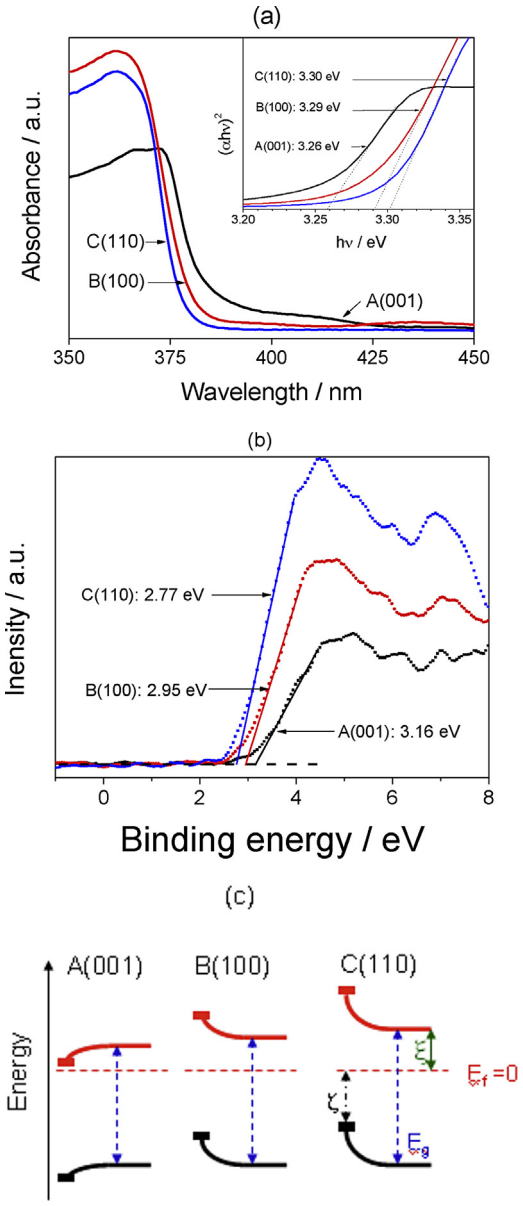

Fig. 3. UV–vis absorption spectra absorption spectra (a), VB-XPS (b) and diagram of band structure (c) of $A(0\,0\,1)$, $B(1\,0\,0)$ and $C(1\,1\,0)$. The inset of a is the plot of $(\alpha h\nu)^2$ vs. $h\nu$.

difference was thought to come from the different preparation of samples.

Taking the optical band gap into account, the Fermi level at all tested samples lied under the conduction band. The surface band bending V_{bb} could be calculated from $V_{bb} = E_g - \zeta - \xi$, as given in Table 1, where $\zeta = E_v - E_F$ is the energy difference between the Fermi level and the VB top in the surface of sample, $\xi = (kT/q)\ln(N_c/n)$ the energy difference between the Fermi level and the conduction band minimum in the bulk of the sample [N_c is the conduction band effective density of states $= 2.94 \times 10^{18}$ cm^{-3} for ZnO using $N_c = 2(2\pi m_e^* kT/h^2)^{3/2}$ and an effective electron mass $m_e^* = 0.24 m_e$],

Table 1
Lattice parameter, thickness, carrier density, ζ, ξ and V_{bb}.

Samples	*a*/*c*-axis (Å)	d_{El} (nm)	n (10^{17})	$\zeta = E_v - E_f$	ξ	V_{bb}
ZnO/Sap(a)	5.2096	268	1.15	3.16	0.084	0.016
ZnO/Sap(m)	3.2598	273	18.74	2.95	0.012	0.328
ZnO/Sap(r)	3.2528	285	17.03	2.77	0.014	0.516

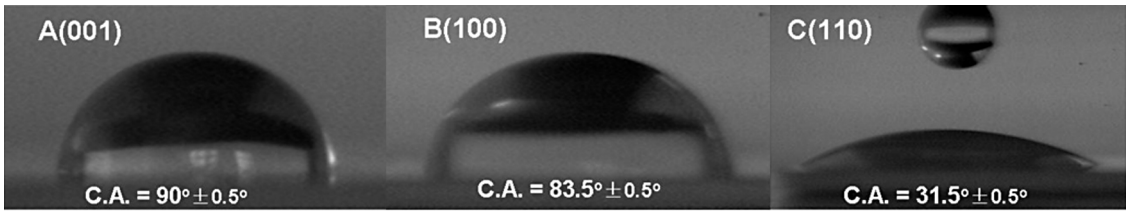

Fig. 4. Contact angle obtained from $A(0\,0\,1)$, $B(1\,0\,0)$ and $C(1\,1\,0)$.

n is the carrier density as shown in Table 1 [23]. Compared V_{bb} with ξ, it could be seen that the $A(0\,0\,1)$ had the downward band bending, whereas the $B(1\,0\,0)$ and $(1\,1\,0)$ had the upward band bending, as shown in Fig. 3c. The photogenerated hole and electron induced oxidation and reduction on the same crystal planes, the upwards surface band bending probably increased the oxidation ability of holes. The dye was easy to be oxidized by the oxidized species coming from the photogenerated holes, such as •OH. Also the photogenerated electrons would do some contribution to the formation of •OH via a series of reactions in liquid [24].

The positions of surface band bending became more negative in the order of $A(0\,0\,1) > B(1\,0\,0) > C(1\,1\,0)$. Moreover, the more negative the positions of surface band bending are, the higher the photocatalytic activity is. The difference between the band position and the energy level of the oxidized radical played an important role in the photocatalytic reaction. The $O_2^{\bullet-}$ and •OH were two main oxidized species for the dye decomposition, of which the energy levels at pH 7 were −0.28 and 2.27 eV vs. NHE [25]. Zhao et al. found that a two-fold rate attenuation was observed when a radical scavenger, dimethyl sulfoxide, was added to a MB solution containing the ZnO nanoplates composed with $(0\,0\,1)$ and $(1\,0\,0)$ plane, which implies that the positions of surface band bending for $(0\,0\,1)$ and $(1\,0\,0)$ straddle the energy levels of $O_2^{\bullet-}$ and •OH [26]. Moreover, the position of surface band bending for C$(1\,1\,0)$ was the most negative in all tested samples. Thus, the positions of surface band bending for all tested samples straddled the energy levels of $O_2^{\bullet-}$ and •OH. Consequently, the appropriate and large difference in the positions of surface band bending and energy levels of the oxidized radicals in $C(1\,1\,0)$ possibly brought the highest photocatalytic activity.

Usually, surface morphology and roughness could affect the photocatalytic activity as well. From the SEM images (see Fig. S3 in Supporting information), $A(0\,0\,1)$ and $B(1\,0\,0)$ showed the surface with some holes with different size which could be caused by the island-like growth; $C(1\,1\,0)$ exhibited the surface with some particles. AFM images showed that all samples were composed with the sphere particles (see Fig. S3 in Supporting information). The average roughness was estimated to be 1.1 nm for $A(0\,0\,1)$, 0.7 nm for $B(1\,0\,0)$ and 0.6 nm for $C(1\,1\,0)$. Generally, the rough surface would offer larger contact area between the solid surface and liquid solution, possibly generating more active sites for photocatalytic reaction. However, in our case the activity seemed to be opposite to the roughness. In addition, the difference in roughness was so small. Consequently, roughness was not considered to be the important factor for the difference in the photocatalytic activity.

Surface free energy could be evaluated from the contact angle measurement because they did not have the special microstructure. Generally, the smaller the contact angle is, the higher the surface free energy is. The results of contact angle measurement for all the tested samples were shown in Fig. 4. The contact angle decreased with the order of $A(0\,0\,1) > B(1\,0\,0) > C(1\,1\,0)$, which revealed that the surface free energy increased with the order of $A(0\,0\,1) < B(1\,0\,0) < C(1\,1\,0)$. Meyer et al. reported the calculation results that the energy of the $(1\,1\,0)$ surface was only slightly higher than that of the $(1\,0\,0)$ surface, but much lower than these of the two polar ZnO surfaces [27]. However, Sun et al. found the ZnO film with $(0\,0\,2)$ face showed the contact angle of ∼109° [28]. Consequently, the present results were considered reasonable. Furthermore, Bi et al. proposed that the higher photocatalytic activity of Ag_3PO_4 could be obtained in the sample exposed the face with the higher surface energy [29]. The fact that the same order of surface free energy as that of photocatalytic activity demonstrated that the surface free energy was closely relative to the photocatalytic activity.

Surface conductivity, especially under light irradiation, was very important to the photoelectric processing in semiconductor. The surface conductivity in the dark and under full arc of Xe lamp irradiation was measured. The conductivity under light irradiation was larger than that in the dark (see Fig. S4 in Supporting information), which was consistent with the previous report [30]. Moreover, the rate constants for MO and DCP degradation increased nearly linearly with the increase in the conductivity under light irradiation, as shown in Fig. 5. The light irradiation would bring the much larger electron mobility than that in the dark [30]. The larger mobility would bring the faster electron transfer and reduction of the combination rate, resulting in a higher activity. It was thus reasonable to understand that the $C(1\,1\,0)$ with the larger conductivity showed the higher activity, implying that improving the conductance could be a good way to obtain the higher activity.

The Raman spectra were shown in Fig. 6a. Except for the peaks of substrate (see Fig. S5 in Supporting information), the new peak at 644 cm^{-1} was observed in the three samples and the new peak at 354 cm^{-1} was obtained in $A(0\,0\,1)$. The peak at 644 cm^{-1} was also observed in N-doped ZnO, [31] Ga and N codoped ZnO, [32] Fe, Sb, Al and Ga doped ZnO, [33] and Mn and Co codoped ZnO [34]. Kaschner [31] and Hasuike [32] proposed that the peak were ascribed to local vibration modes due to nitrogen-related complexes, but Du et al. [34] attributed it to the Zn interstitials or oxygen vacancies based on the fact that the peak disappeared with the increase of annealing temperature and time. Our specimens did not contain nitrogen, consequently, it could not come from the local vibration modes relating to nitrogen-related complexes. Therefore, the peak at 644 cm^{-1} was possibly attributed to the defects, although the precise type of defects was not clear. Furthermore, the normalized

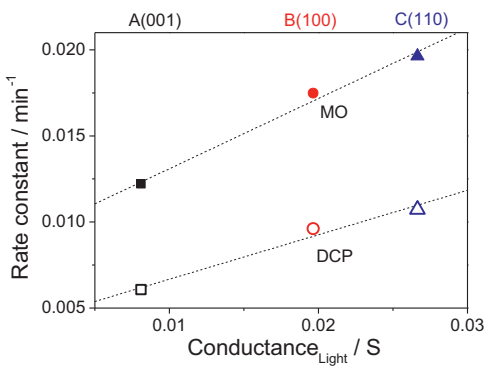

Fig. 5. Variation in surface conductivity of $A(0\,0\,1)$, $B(1\,0\,0)$ and $C(1\,1\,0)$ under full arc of Xe lamp irradiation.

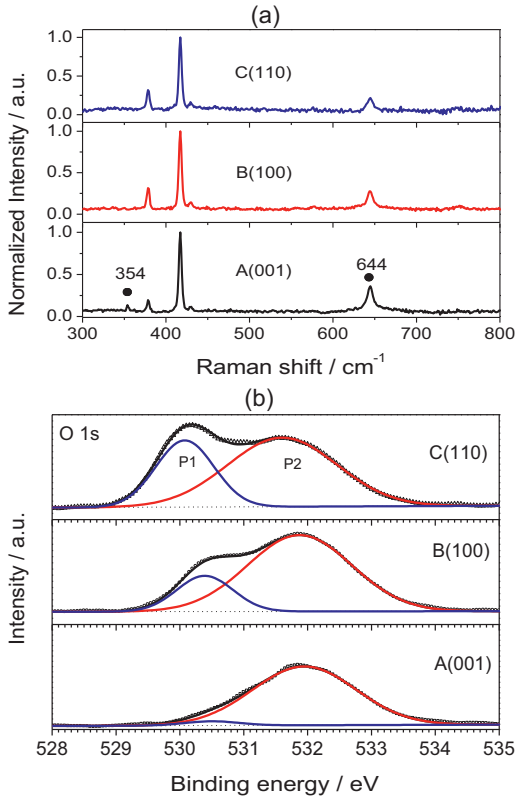

Fig. 6. Raman spectra (a), and O 1s (b) XPS line obtained from $A(0\,0\,1)$, $B(1\,0\,0)$ and $C(1\,1\,0)$. The black dot marks the peak of ZnO. The excitation wavelength of the Raman spectra is 632 nm.

intensity at 644 cm^{-1} (normalized to the peak at 417) decreased in the order of $A(0\,0\,1) > B(1\,0\,0) > C(1\,1\,0)$, implying that the amount of the defects decreased with the order of $A(0\,0\,1) > B(1\,0\,0) > C(1\,1\,0)$, though the exact amount was still undetermined.

XPS analysis was employed to determine surface chemical composition of as-obtained ZnO films. The Zn was oxide state (see Fig. S6 and Table SI in Supporting information). The fitting of O 1s region with two-peak contribution indicated that at least two kinds of oxygen species were present in the near surface domain of the ZnO films, as shown in Fig. 6b. The peak P1 at about 530 eV was due to crystal lattice oxygen of ZnO, while the peak P2 at about 531.9 eV was due to chemisorbed oxygen on the film surface [35,36]. The area of P2 (S_{P2}) was in the same magnitude for three samples, but that of P1 (S_{P1}) increased obviously with the order of $A(0\,0\,1) < B(1\,0\,0) < C(1\,1\,0)$. The relative ratio of S_{P1} to S_{P2} increased with the order of $A(0\,0\,1) < B(1\,0\,0) < C(1\,1\,0)$. Lee et al. found that the O 1s XPS line in the Al-doped ZnO also only had the peak of 532 eV, but the peak of 532 and 530 eV could coexist after 40 nm sputter-etching [36]. These previous studies implied that the surface adsorbed oxygen could shade the signal of crystal lattice oxygen. The more the adsorbed oxygen is, the weaker the signal of crystal lattice oxygen. Wang et al. thought that the peak at 531.8 eV in O 1s XPS line in the ZnO prepared from the precursor of Zn_2O was associated with O^{2-} in the oxygen deficient regions with the matrix of ZnO, and the intensity of this peak was connected to the concentration of oxygen vacancies [37]. Consequently, we suggested herein that the amount of the defects increased with the order of $A(0\,0\,1) > B(1\,0\,0) > C(1\,1\,0)$. Although some recent works showed that the defect was very important to the photocatalytic activity, our results indicated that the defect did not show the positive effect [37,38]. The $A(0\,0\,1)$ sample contained the most amount of defects, but its activity was the lowest. Consequently, we considered other properties as the reason for the different photocatalytic activity among three samples. Also we found the oriented (0 0 1) samples on a and c-face sapphire showed the same phenomenon. The more amount of the defect the sample contains, the lower photocatalytic activity the sample shows. Some researchers proposed that there was an optimum amount of defect on surface and bulk for the best photocatalytic performance [39]. Unfortunately, in our case, our samples fell in the downward part.

4. Conclusions

In summary, we demonstrated that the ZnO showed the anisotropy in the photocatalytic activity. This anisotropy was ascribed to the difference in the surface band bending, adsorption property, surface free energy and surface conductivity. Additionally, it was the first time to find that the (1 1 0) crystal plane showed the highest activity in the three low-indexed crystal planes. These results would be valuable for further investigation of ZnO.

Acknowledgements

This work was supported by the National Natural Science Foundation of China (21103041), National Postdoctoral Funding (2011M500786), and Program for Innovative Research Team in Science and Technology in University of Henan Province (IRTSTHN) (Grant No. 2012 IRTSTHN004).

Appendix A. Supplementary data

Supplementary data associated with this article can be found, in the online version, at http://dx.doi.org/10.1016/j.apcatb.2014.04.034.

References

[1] N. Serpone, A.V. Emeline, J. Phys. Chem. Lett. 3 (2012) 673–677.
[2] A. Kudo, Y. Miseki, Chem. Soc. Rev. 38 (2009) 253–278.
[3] G. Liu, J.C. Yu, G.Q. Lu, H.M. Cheng, Chem. Commun. (Camb.) 47 (2011) 6763–6783.
[4] F.E. Osterloh, Chem. Soc. Rev. 42 (2013) 2294–2320.
[5] H. Tong, S. Ouyang, Y. Bi, N. Umezawa, M. Oshikiri, J. Ye, Adv. Mater. 24 (2012) 229–251.
[6] E.S. Jang, J.H. Won, S.J. Hwang, J.H. Choy, Adv. Mater. 18 (2006) 3309–3312.
[7] N. Kislov, J. Lahiri, H. Verma, D.Y. Goswami, E. Stefanakos, M. Batzill, Langmuir 25 (2009) 3310–3315.
[8] A. Mclaren, T. Valdes-Solis, G.Q. Li, S.C. Tsang, J. Am. Chem. Soc. 131 (2009) 12540–12541.
[9] M.Y. Guo, A.M.C. Ng, F. Liu, A.B. Djurišić, W.K. Chan, H. Su, K.S. Wong, J. Phys. Chem. C 115 (2011) 11095–11101.
[10] J. Gupta, K.C. Barick, D. Bahadur, J. Alloys Compd. 509 (2011) 6725–6730.
[11] T. Tachikawa, S. Yamashita, T. Majima, J Am. Chem. Soc. 133 (2011) 7197–7204.
[12] M. Miyauchi, A. Shimai, Y. Tsuru, J. Phys. Chem. B 109 (2005) 13307–13311.
[13] W. Wang, G. Li, N. Yang, W. Zhang, Mater. Chem. Phys. 123 (2010) 322–325.
[14] J.M. Chauveau, P. Vennéguès, M. Laügt, C. Deparis, J. Zuniga-Perez, C. Morhain, J. Appl. Phys. 104 (2008) 073535.
[15] P. Ding, X.H. Pan, J.Y. Huang, H.P. He, B. Lu, H.H. Zhang, Z.Z. Ye, J. Cryst. Growth 331 (2011) 15–17.
[16] S.L. King, J.G.E. Gardeniers, I.W. Boyd, Appl. Surf. Sci. 96–98 (1996) 811–818.
[17] L. Schmidt-Mende, J.L. MacManus-Driscoll, Mater. Today 10 (2007) 40–48.
[18] R. Dom, H.G. Kim, P.H. Borse, CrystEngComm (2014), http://dx.doi.org/10.1039/c3ce42058b.
[19] G. Li, T. Kako, D. Wang, Z. Zou, J. Ye, J. Solid State Chem. 180 (2007) 2845–2850.
[20] G. Li, N. Yang, W. Wang, W.F. Zhang, Electrochim. Acta 55 (2010) 7235–7239.
[21] S. Ouyang, H. Tong, N. Umezawa, J. Cao, P. Li, Y. Bi, Y. Zhang, J. Ye, J. Am. Chem. Soc. 134 (2012) 1974–1977.
[22] A.L. Yang, H.P. Song, H.Y. Wei, X.L. Liu, J. Wang, X.Q. Lv, P. Jin, S.Y. Yang, Q.S. Zhu, Z.G. Wang, Appl. Phys. Lett. 94 (2009) 163301.
[23] M.W. Allen, C.H. Swartz, T.H. Myers, T.D. Veal, C.F. McConville, S.M. Durbin, Phys. Rev. B 81 (2010) 075211.
[24] H. Kisch, Angew. Chem. 52 (2013) 812–847.
[25] A. Fujishima, T.N. Rao, D.A. Tryk, J. Photochem. Photobiol. C: Photochem. Rev. 1 (2000) 1–21.
[26] Y. Zhao, C. Eley, J. Hu, J.S. Foord, L. Ye, H. He, S.C.E. Tsang, Angew. Chem. Int. Ed. 51 (2012) 3846–3849.
[27] B. Meyer, D. Marx, Phys. Rev. B 67 (2003) 035403.

[28] R. Sun, A. Nakajima, A. Fujishima, T. Watanabe, K. Hashimoto, J. Phys. Chem. B 105 (2001) 1984–1990.
[29] Y. Bi, S. Ouyang, N. Umezawa, J. Cao, J. Ye, J. Am. Chem. Soc. 133 (2011) 6490–6492.
[30] C.H. Swartz, J. Mater. Res. 27 (2012) 2205–2213.
[31] A. Kaschner, U. Haboeck, M. Strassburg, M. Strassburg, G. Kaczmarczyk, A. Hoffmann, C. Thomsen, A. Zeuner, H.R. Alves, D.M. Hofmann, B.K. Meyer, Appl. Phys. Lett. 80 (2002) 1909.
[32] N. Hasuike, H. Fukumura, H. Harima, K. Kisoda, H. Matsui, H. Saeki, H. Tabata, J. Phys.: Condens. Matter 16 (2004) S5807–S5810.
[33] C. Bundesmann, N. Ashkenov, M. Schubert, D. Spemann, T. Butz, E.M. Kaidashev, M. Lorenz, M. Grundmann, Appl. Phys. Lett. 83 (2003) 1974.
[34] C.L. Du, Z.B. Gu, M.H. Lu, J. Wang, S.T. Zhang, J. Zhao, G.X. Cheng, H. Heng, Y.F. Chen, J. Appl. Phys. 99 (2006) 123515.
[35] Y. Du, Y. Zhang, L. Sun, C. Yan, J. Phys. Chem. C 112 (2008) 12234–12241.
[36] D. Lee, O. Kwon, J. Song, C. Park, K. Park, S. Nam, Y. Kim, Solar Energy Mater. Solar Cells 105 (2012) 15–20.
[37] J. Wang, Z. Wang, B. Huang, Y. Ma, Y. Liu, X. Qin, X. Zhang, Y. Dai, ACS Appl. Mater. Interfaces 4 (2012) 4024–4030.
[38] Y. Wang, H. Sun, S. Tan, H. Feng, Z. Cheng, J. Zhao, A. Zhao, B. Wang, Y. Luo, J. Yang, J.G. Hou, Nat. Commun. 4 (2013) 2214.
[39] M. Kong, Y. Li, X. Chen, T. Tian, P. Fang, F. Zheng, X. Zhao, J. Am. Chem. Soc. 133 (2011) 16414–16417.